Cu-BTC-based composite adsorbents for selective adsorption of CO2 from syngas

Zhang Yan, Wibowo Haryo, Zhong Li, Horttanainen Mika, Wang Zunbo, Yu Caimeng, Yan Mi

DOI: 10.1016/j.seppur.2021.119644

Cu-BTC-based composite adsorbents for selective adsorption of CO_2 from syngas

Yan Zhang[a], Haryo Wibowo[a], Li Zhong[b], Mika Horttanainen[c], Zunbo Wang[a], Caimeng Yu[d], Mi Yan [a]*

[a] *Institute of Energy and Power Engineering, Zhejiang University of Technology, Hangzhou 310014, China*

[b] *Huaneng Yangtze Environmental Technology Co. Ltd, Beijing 102209, China*

[c] *Department of Sustainability Science, Lappeenranta University of Technology, Lappeenranta 3453850, Finland*

[d] *Zhejiang Zheneng Xingyuan Energy Saving Technology Co. Ltd, Hangzhou 310013, China*

**Corresponding author: Mi Yan (E-mail: yanmi1985@zjut.edu.cn)*

Highlight

- Modification of Cu-BTC with Mg^{2+} and MWCNT to produce high performance composite adsorbent.
- CO_2 adsorption performances of Mg/Cu-BTC@MWCNT were evaluated.
- High selectivity of CO_2 from syngas was achieved.

Graphical Abstract:

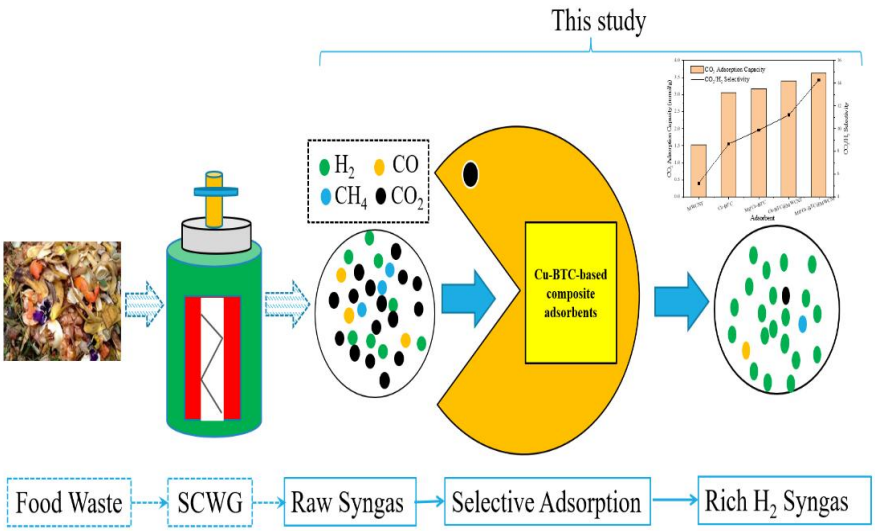

Abstract

High CO_2 content exists in the raw syngas produced from supercritical water gasification of food waste, CO_2 removal to improve quality of the syngas is necessary before further utilization. In this study, Cu-BTC, Mg/Cu-BTC, Cu-BTC@MWCNT, and Mg/Cu-BTC@MWCNT were synthesized and characterized as CO_2 adsorbents. The adsorption experiments were conducted to investigate the optimal adsorbent and adsorption conditions. The results indicated that Mg^{2+} and multi-walled carbon nanotubes (MWCNT) doped into Cu-BTC influenced the physical properties of adsorbents. Among of all studied adsorbents, Mg/Cu-BTC@MWCNT had the maximum CO_2 adsorption capacity (3.63 mmol/g) and selectivity (14.28) at 25 °C and 100 kPa. Analysis of variance (ANOVA) exhibited that adsorption pressure had significant effects on CO_2 adsorption capacity of Mg/Cu-BTC@MWCNT. The influences of different operating parameters on CO_2 adsorption capacity and selectivity were discussed in Mg/Cu-BTC@MWCNT. The adsorption isotherms of gas components on Mg/Cu-BTC@MWCNT can be sorted as follows: CO_2 > CO> CH_4 >H_2. In additional, the regeneration experiment with 5 times was conducted and the result showed that Mg/Cu-BTC@MWCNT has high stability.

Keyword: Cu-BTC, multi-walled carbon nanotubes, CO_2 adsorption, selectivity, syngas

1. Introduction

Approximately 1.3 billion tons of the food waste is generated every year in the world [1]. Traditional technologies such as landfill and incineration to dispose food waste with high water content have some limitations, especially in terms of efficient energy consumption and environment pollution [2]. Supercritical water gasification (SCWG) can to effectively convert high humidity food waste into combustible syngas. However, one main drawback of this method is high content of CO_2 produced in raw syngas, which could be around 35% to 50% of the total volume [3]. The presence of CO_2 could reduce the heating value and limit applications of syngas as chemical feedstocks [4]. Therefore, to improve the quality of syngas and reduce greenhouse gas emissions, it is of particular importance to investigate suitable technologies to remove CO_2 for desirable syngas.

Commonly used techniques of CO_2 capture include chemical absorption and physical adsorption [5], [6]. Amine solutions such as mono-ethanolamine (MEA) and

diethanolamine (DEA) are the most widely used industrial chemical absorbent for CO_2 absorption [7], [8]. While, the use of amine solution can cause equipment corrosion. Regeneration of used amine solution requires lots of energy due to the high latent heat of vaporization, some amine also prone to vaporizing during regeneration by heating, making the cost of amine adsorption process for CO_2 is high [9], [10]. Meanwhile, solid porous adsorbents for CO_2 capture can overcome the drawback of amine solutions. Conventional adsorbents such as activated carbon, zeolites 5A, and activated alumina have been extensively studied for use in CO_2 capture and storage [11], [12], [13]. Researches in the past decades have found that metal-organic framework (MOF) have great potential for CO_2 capture and separation owing to its structural adjustability, high adsorption capacity, selectivity, and thermodynamic stability [14], [15]. Copper benzene-1,3,5-tricarboxylate (Cu-BTC) with regular octahedral structure has large BET surface area, high porosity, and the Lewis's acidity of open metal sites, which has led it to be regarded as a promising adsorbent for gas adsorption [16], [17]. However, the hydrophilicity of Cu-BTC resulted in structural damage and poor adsorption when exposed to gas containing water vapor [18], [19]. For addressing this weakness, previous studies have shown the structure and characteristics of Cu-BTC could be changed by modifying coordination bonds-based connections between its organic linkers and metal-containing nodes [20], [21], [22].

Ion doping and functional group modification are good methods to enhance water resistance and CO_2 adsorption performance of Cu-BTC [23], [24]. Mg-MOF-74 membrane has outstanding performance in both CO_2 adsorption capacity of 380 mg CO_2/g and H_2/CO_2 selectivity of 10.5 at 25 °C, which is attributed to the free interaction of unsaturated Mg center sites with CO_2. [25]. Cu-BTC dopped with alkali metals (Li, Na and K) have a higher CO_2 adsorption capacity and CO_2/N_2 selectivity [26]. In order to further enhance the CO_2 adsorption performance of Cu-BTC, multi-walled carbon nanotube (MWCNT) was used to functionalize Cu-BTC. MWCNT with carboxylic groups (-COOH) is a kind of light-weight hydrophobic material with high specific surface area. It also has excellent thermal and electrical conductivity [27], [28]. The introduction of functional groups (-COOH) into the material can adjust its polarity and acidity, enhancing affinity to CO_2 [29]. MWCNT-modified MOF has some advantages

such as good dispersibility and high hydrophobicity, which are expected to increase the gas adsorption rate and reduce water sensitivity of MOF [30], [31]. Yang et al. [32] found that MOF-5 modified by CNT greatly improved the moisture stability under ambient conditions. Eshraghi et al. [33] reported that the CO_2 adsorption capacity of MWCNT/MIL-100 and MWCNT/Cu-BTC increased to 4.3 mmol/g and 2.9 mmol/g compared with Cu-BTC (0.9 mmol/g), respectively. This was due to the increase of micropore volume of MWCNT incorporated MOF. Xiang et al. [34] developed the hybrid composite material of MWCNT/Cu-BTC doping of lithium ions, which resulted in an improvement of the CO_2 and CH_4 adsorption capacity by 305% and 200%, compared to only Cu-BTC. However, the knowledge of Mg^{2+} and MWCNT doping Cu-BTC on syngas upgrading is lacking.

Based on mentioned current research and drawback, this work mainly investigated the influence of incorporating Mg^{2+} and MWCNT into Cu-BTC on its CO_2 adsorption capacity and selectivity from raw syngas of SCWG, for creating the optimal adsorbent and adsorption conditions.

2. Experimental section

2. 1. Synthesis of Cu-BTC-based composite adsorbents

All reagents were purchased from Aladdin (Shanghai, China), including copper nitrate trihydrate ($Cu(NO_3)_2 \cdot 3H_2O$, 99%), magnesium nitrate hexahydrate ($Mg(NO_3)_2 \cdot 6H_2O$, 99%), benzene-1,3,5-tricarboxylic acid (H_3BTC, 95%), N, N-Dimethylformamide (DMF, 99.8%), nitric acid (HNO_3, 99%) and ethanol (99.7%) and multi-walled carbon nanotube (MWCNT). These chemicals were analytical reagent grade and used without further purification.

Synthesis of Cu-BTC was performed following the reported procedures by Janabi et al. [35] with some modifications. First, 2 g of $Cu(NO_3) \cdot 3H_2O$ and 1 g of H_3BTC were immersed in a mixture of deionized water/ethanol/DMF (1:1:1). The mixture was stirred until complete dissolution. Then, they were transferred to a 100 ml (Teflon-stainless steel) autoclave and heated at 100 °C for 48 h. After the heating process was completed and the sample was cooled to room temperature, the resulting blue precipitate was washed with deionized water and ethanol three times to remove impurities. Finally, the synthesized adsorbent was dried at 120 °C for 8 h in a vacuum oven to obtain fine Cu-BTC powder.

For the preparation of Mg/Cu-BTC, the synthesis process was similar to the synthesis of Cu-BTC. The difference was that $Cu(NO_3)\cdot 3H_2O$ and $Mg(NO_3)_2\cdot 6H_2O$ were added to the mixture solution at a molar ratio of 4:1. The other steps were remained. The product of this process was denoted as Mg/Cu-BTC.

Before MWCNT was used to functionalize Cu-BTC and Mg/Cu-BTC, MWCNT was acidified with HNO_3. The purpose is to introduce carboxyl groups (-COOH) on the surface of MWCNT and remove impurities. MWCNT with -COOH supported a continuous copper framework growth by providing uniform nucleation sites. First, the synthesis step involved dispersing 1 g MWCNT in 50 ml HNO_3 using ultrasonication. The mixed solution was transferred to a 100 ml round bottom flask and was refluxed by a rotary evaporator at 110 °C for 24 h. After filtration, the mixture was washed repeatedly with deionized water till the pH of the filtrate reached approximately 5.5. Finally, the adsorbent was dried at 80 °C and ground into fine powder.

The synthesis of MWCNT@Cu-BTC and Mg-MWCNT@Cu-BTC employed the pre-synthesis modification method. Compare to post-synthesis, the pre-synthesis operation is simpler and better for activated adsorbent, it also results in less quality loss. First, 0.4 g MWCNT was separately added to either 2 g Cu-BTC or 2 g Mg/Cu-BTC solution and each mixture was stirred for 30 min. Then each solution was placed in a 100 ml Teflon-stainless steel autoclave and was heated 100 °C for 48 h. After reaction completion, the solid product was filtered and washed with anhydrous toluene and ethanol. Finally, the adsorbent was dried at 120 °C for 8 h. The synthesis process of Cu-BTC-based adsorbents described in the previous paragraphs was shown in Fig.1.

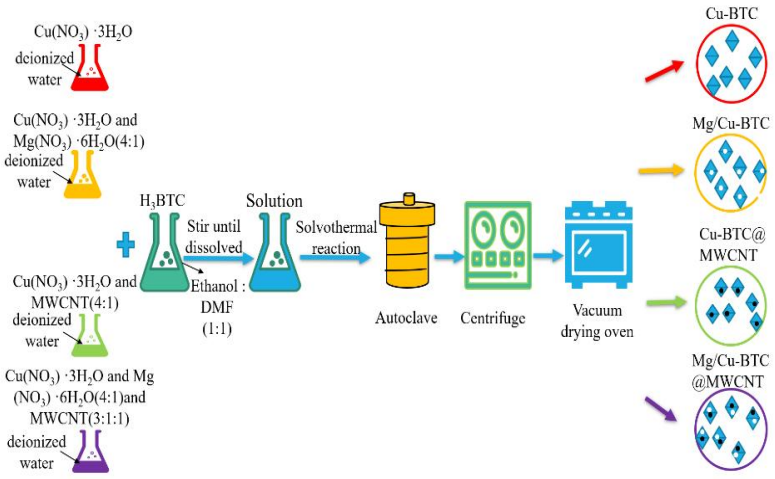

Fig.1. Synthesis procedure of Cu-BTC-based composite adsorbents.

2.2. Characterization

The pore properties of adsorbents were measured by N_2 adsorption/desorption isotherms at -196 °C using Micromeritics Tristar 3020 instrument. The physical properties analyzed include: BET surface area, pore volume, and average pore size. Characterizations of elemental C, Cu, and Mg^{2+} were obtained using a scanning XPS microprobe (PHI Versa Probe III).

2.3. Gas adsorption and measurement

The measurement of the syngas adsorption at different temperatures and pressures was performed in a static volumetric apparatus, shown in Fig.2.

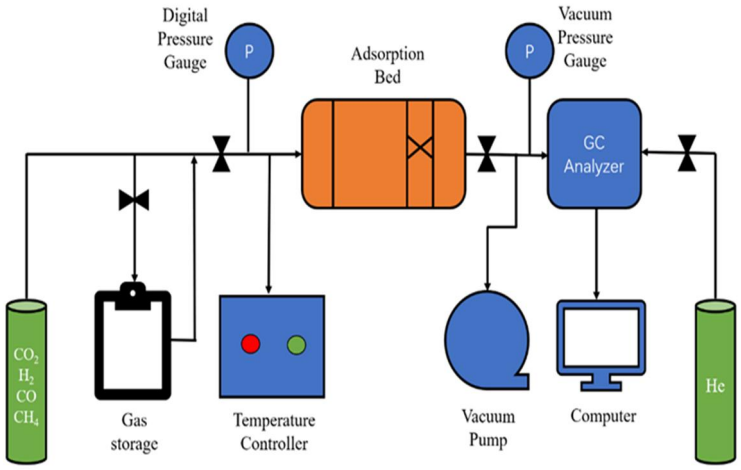

Fig.2. Schematic diagram of syngas adsorption apparatus.

First, the adsorbent was placed in the adsorption bed and packed tightly. After that, the system was fully vacuumed to remove air. The model syngas (40%H_2, 5%CO, 15% CH_4, and 40%CO_2) was then introduced into the system and the pressure was recorded. During the adsorption experiment, gas chromatograph with thermal conductivity detector (GC-TCD) was used to measure the outlet gas composition at 5 min intervals until equilibrium was reached. The adsorption capacity was calculated by the difference of pressure using the ideal gas law by Eq. (1):

$$\Delta n = \frac{\Delta PV}{RT} \quad (1)$$

Where, Δn (mmol) and ΔP (Pa) represent the change of the amount of molar and pressure before and after adsorption; V (m^3) represents the total volume of the system; R (0.008314 J/mmol·K) represents the molar gas constant, and T (K) represents operating temperature.

The selectivity of CO_2/H_2 and $(CO_2+CO+CH_4)/H_2$ can be defined as follows by

Eq. (2):

$$S_{1,2} = \frac{n_1 p_2}{n_2 p_1} \quad (2)$$

Where, n_1 and n_2 (mmol) are adsorption capacity in the syngas at equilibrium, p_1 and p_2 (kPa) are the partial pressure of the gas in the initial state.

3. Result and discussion

3.1. Comparison of synthesized Cu-BTC-based adsorbents

3.1.1. Characterization

N_2 adsorption/desorption isotherms of adsorbents were displayed in Fig.3. According to the classification of the international Union of Pure and Applied Chemistry (IUPAC) [6], the isotherm curve of MWCNT is type III with a clear hysteresis. The adsorption curve increased sharply at low pressure (relative pressure at 0-0.2), which implied the existence of micropores within the network. The N_2 adsorption behavior over MWCNT (relative pressure at 0.8-1.0) can be attributed to the phenomenon of mild capillary condensation into the interparticle voids. A small hysteresis loop demonstrated the existence of a multilayer adsorption. Generally, multilayer adsorption took place in the mesopores in accordance with the Langmuir theory [36]. MWCNT has a mesoporous structure, which is also in good agreement with the measured average pore diameter of 5.74 nm. The N_2 adsorption and desorption curves of Cu-BTC, Mg/Cu-BTC, Cu-BTC@MWCNT, and Mg/Cu-BTC@MWCNT were nearly vertical in low-pressure range, it had a strong affinity between the adsorbent and N_2 molecule. The adsorption isotherm of Cu-BTC is type I adsorption, it is the result of Langmuir single-layer reversible adsorption, indicating that Cu-BTC is mainly microporous material. However, there were hysteresis loops of different sizes in Mg/Cu-BTC, Cu-BTC@MWCNT, and Mg/Cu-BTC@MWCNT. This was because that different volume amounts of mesopores existed in different adsorbents, multi-layer adsorption or capillary condensation caused the delay of N_2 removal during desorption [37]. In all, adsorbent modifications with Mg^{2+} and MWCNT changed the pore structure of the composite adsorbents.

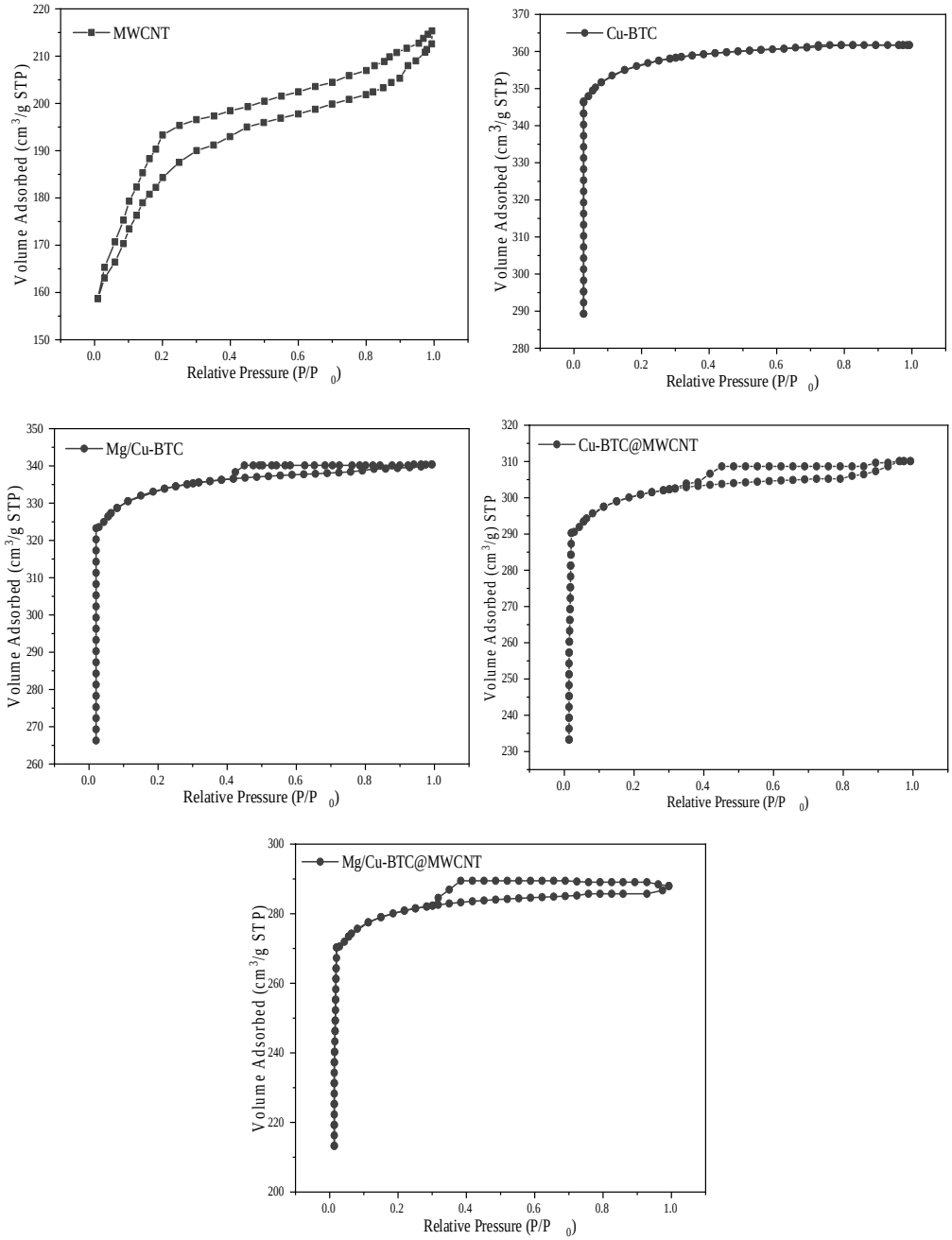

Fig.3. N_2 adsorption/desorption isotherms for MWCNT, Cu-BTC, Mg/Cu-BTC, Cu-BTC@MWCNT, and Mg/Cu-BTC@MWCNT.

The physical properties of adsorbents were listed in Table 1. The BET surface area and pore volume of MWCNT were found to be 354 m^2/g and 0.4 m^3/g. Cu-BTC had the maximum surface area of 1594 m^2/g among five adsorbents, while its total pore volume and microporous volume were determined to be 0.64 and 0.52 m^3/g, respectively. Compared to Cu-BTC, the surface area and pore volume of Mg/Cu-BTC, Cu-BTC@MWCNT, and Mg/Cu-BTC@MWCNT had lower surface area and pore

volume. However, their micropores proportions were enhanced slightly, it might be attributed to the structural regulation effect of Mg^{2+} and MWCNT on the internal structure of Cu-BTC. The increase of the average pore size exhibited some extent of pore blockage during the doping Mg^{2+} or MWCNT into Cu-BTC.

Table 1. Textural properties of adsorbents from N_2 adsorption/desorption isotherms.

Adsorbent	S_{BET} (m^2/g)	V_{total} (m^3/g)	V_{micro} (m^3/g)	V_{micro}/V_{total}	D_{APD} (nm)
MWCNT	354	0.4	0.23	0.57	5.74
Cu-BTC	1594	0.64	0.52	0.81	1.53
Mg/Cu-BTC	1459	0.6	0.48	0.8	1.6
Cu-BTC@MWCNT	1150	0.55	0.46	0.83	1.72
Mg/Cu-BTC@MWCNT	1424	0.57	0.49	0.86	1.55

The XPS spectra of adsorbents were presented in Fig.4. The peaks of MWCNT showed distinct carbon and oxygen peaks, which were around 285 and 533 eV [38]. For Cu-BTC, Mg/Cu-BTC, Cu-BTC@MWCNT, and Mg/Cu-BTC@MWCNT, XPS analysis displayed two main peaks of Cu $2p_{2/3}$ and Cu $2p_{1/2}$ located at 934.3 eV and 953.1 eV, which were representative of Cu-BTC-CO and Cu-BTC-O [37]. This showed that the addition of Mg^{2+} and MWCNT did not affect the coordination bonds between Cu and BTC. A few peaks between 932.3 eV and 940.5 eV were the appearance of Cu_2O and CuO. For Mg/Cu-BTC and Mg/Cu-BTC@MWCNT, the peak around 49.7 eV was Mg^{2+}, which was from $Mg(NO_3)_2$, deposited on the Mg/Cu-BTC and Mg/Cu-BTC@MWCNT. It revealed that Mg^{2+} was successfully added to the adsorbents. Meanwhile, the atomic ratio of Mg can also be seen in Table 2. Cu-BTC@MWCNT and Mg/Cu-BTC@MWCNT existed a peak at 285 eV, which represented C1s. It was worth noting that there was no obvious peak shift or difference that occurred when Cu-BTC were loaded with Mg^{2+} and/ or MWCNT, which indicated that Cu-BTC has good stability.

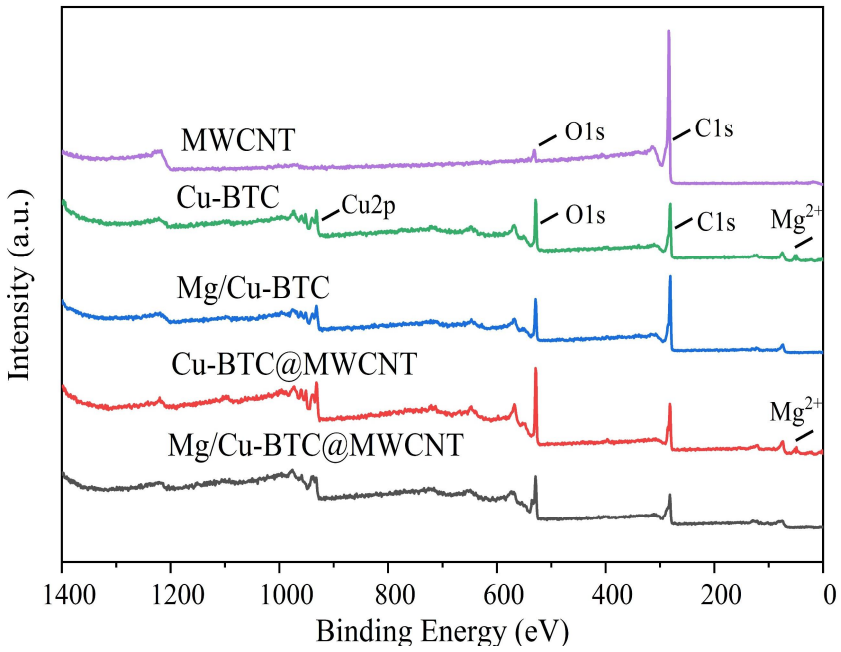

Fig.4. XPS spectra of the MWCNT, Cu-BTC, Mg/Cu-BTC, Cu-BTC@MWCNT, and Mg/Cu-BTC@MWCNT.

Table 2. The atomic ratio of C, Cu, and Mg in adsorbents.

Adsorbent	Atomic ratio (%)		
	C	Cu	Mg
MWCNT	95.72	/	/
Cu-BTC	/	7.82	/
Mg/Cu-BTC	/	10.3	1.5
Cu-BTC@MWCNT	19.88	6.05	/
Mg/Cu-BTC@MWCNT	18.27	7.61	1.37

3.1.2. CO_2 adsorption performance

CO_2 adsorption capacity and CO_2/H_2 selectivity of adsorbents were measured at 25 °C and 100 kPa in Fig.5. MWCNT has a CO_2 adsorption capacity of 1.53 mmol/g. This is not only because MWCNT has a high BET surface area and pore volume, HNO_3 acidification of MWCNT also enhance the interaction between CO_2 and adsorbent [32]. The CO_2 adsorption capacity of Cu-BTC was observed to be at 3.06 mmol/g due to the presence of unsaturated metal sites and large specific surface area. The CO_2 adsorption capacity of Mg/Cu-BTC, Cu-BTC@MWCNT, and Mg/Cu-BTC@MWCNT were 3.7%,

11.1%, and 18.5% higher than the pristine Cu-BTC, respectively. It showed that Mg^{2+} and MWCNT doping increased the adsorption capacity of CO_2 to a certain extent. The positive effect of Cu-BTC doped with Mg^{2+} was because an alkaline metal (Mg) had high affinity to acidic CO_2 molecule, replacing some of the unsaturated sites of Cu. The CO_2 adsorption capacity of Cu-BTC@MWCNT was higher than Mg/Cu-BTC, indicating MWCNT with its high specific surface area and pore volume had a more significant effect than Mg^{2+} in increasing the CO_2 adsorption. From the result, Mg/Cu-BTC@MWCNT had the highest CO_2 adsorption capacity among the studied adsorbents; at 3.63 mmol/g. This could be explained as the synergistic effect of Mg^{2+} and MWCNT on Cu-BTC increased the interaction between CO_2 and adsorbent. Doping of Mg^{2+} into Cu-BTC provided unsaturated metal sites and affected CO_2 adsorption. MWCNT doping into Cu-BTC not only added extra pore volume, but also increased the number of carboxyl group after being treated by nitric acid, this increased the adsorption of CO_2 by the adsorbent.

In addition to discussing CO_2 adsorption capacity, the selectivity of an adsorbent towards CO_2 compared to other gases was also an important property for its effective application. In Fig.5, the order of CO_2/H_2 adsorption selectivity as follows: Mg/Cu-BTC@MWCNT> Cu-BTC@MWCNT> Mg/Cu-BTC> Cu-BTC> MWCNT. The difference in CO_2/H_2 selectivity of Cu-BTC@MWCNT and Mg/Cu-BTC@MWCNT is because the addition of Mg^{2+} into Cu-BTC@MWCNT increased CO_2 adsorption capacity, while it has little effect on the H_2 adsorption capacity. Among them, Mg/Cu-BTC@MWCNT had the highest CO_2/H_2 selectivity at 14.28. Therefore, Mg/Cu-BTC@MWCNT produced both the best adsorption capacity and selectivity among adsorbents. For that reason, Mg/Cu-BTC@MWCNT can be selected for further investigations and discussion in the following sections.

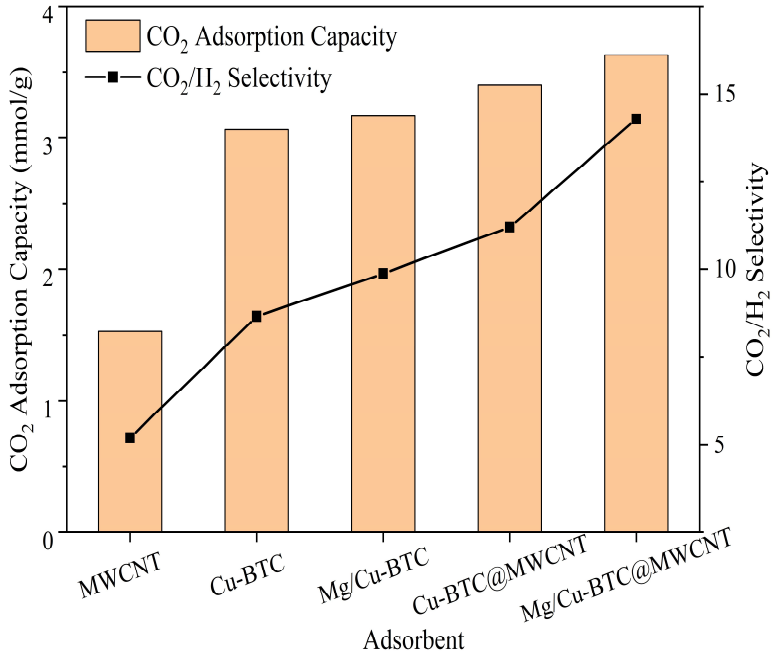

Fig.5. CO_2 adsorption capacity and CO_2/H_2 selectivity of Cu-BTC-based adsorbents at 25 °C and 100 kPa.

3.2. CO_2 adsorption performance of Mg/Cu-BTC@MWCNT

3.2.1. Influence of operating parameters on CO_2 adsorption capacity

CO_2 adsorption isotherms were obtained at different adsorption temperatures and pressures in Fig.6(a) and (b). The CO_2 adsorption capacity at 0 °C and 100 kPa was higher than that at 25 °C and 50 °C by 15.2% and 86.3%, respectively. This was consistent with the result that the CO_2 adsorption by Cu-BTC is an exothermic process [27]. When the adsorption equilibrium is reached, increasing the temperature can inhibit adsorption reaction. With increasing temperature, the thermal movement of gas molecules in the pores of the adsorbent was also accelerated, which would promote the escape of gas molecules from the adsorbent. Lowering adsorption temperature increased CO_2 adsorption capacity. Therefore, it is necessary for the syngas from SCWG or other thermal gasification to be cooled down before CO_2 removal by MOF. This also provide extra benefit as the cool syngas is more suitable for further storage and transportation. Meanwhile, an increase of CO_2 adsorption capacity with increasing pressure was observed. When adsorption pressure increased to 500 kPa, CO_2 adsorption capacity was increased by 32.2% and 110.5% at 25 °C and 50 °C. According to previous studies [39], [40], [41], Cu-BTC is a microporous material, even doped Mg^{2+} and MWCNT, the BET surface area and micropore-volume of Mg/Cu-BTC@MWCNT also

have a strong contribution to CO_2 adsorption capacity. Under low adsorption pressure, gas diffusion primarily happened at the main pores of the adsorbent. By increasing pressure, CO_2 entered directly into the unoccupied spaces including unsaturated metal sites and side pores. These observations suggested that the distribution of pores, especially (V_{micro}/V_{total}), might play a significant contribution in determining the CO_2 adsorption performance of Cu-BTC. From Table 1, The V_{micro}/V_{total} of Mg/Cu-BTC@MWCNT is 0.86, this high value is one reason why it has high CO_2 adsorption. In order to clearly compare the effect of temperature and pressure, some typical cases were compared in Fig.6(c). It can be obviously concluded that low temperature and high pressure is beneficial for CO_2 adsorption, resulting in a maximum adsorption capacity of 20.02 mmol/g.

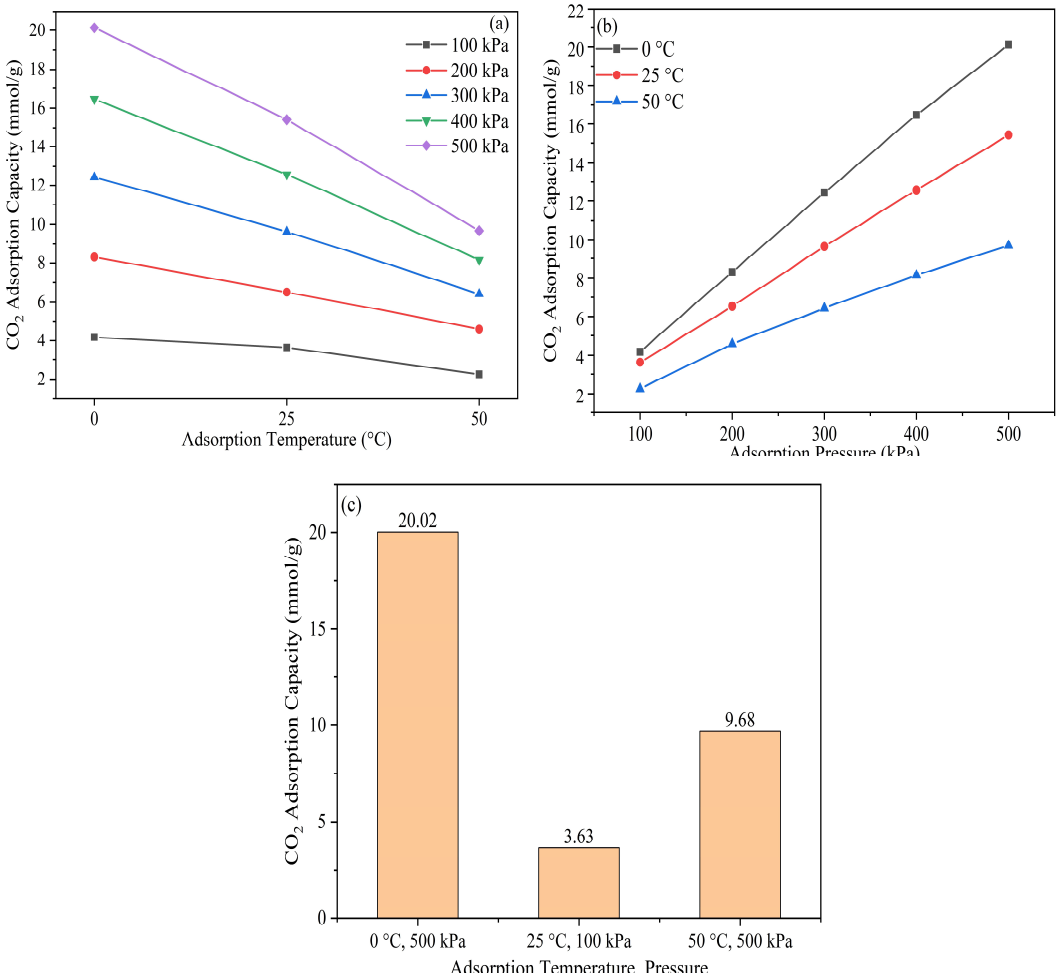

Fig.6. CO_2 adsorption capacity: (a) the effect of adsorption pressure; (b) the effect of adsorption pressure; (c) comparison between low temperature & high pressure (0 °C & 500 kPa), room temperature & room pressure (25 °C & 100 kPa), and high temperature and high pressure (50 °C & 500 kPa).

Compared with other adsorbents in Table 3, Mg/Cu-BTC@MWCNT had more prominent CO_2 adsorption capacity under similar operating conditions. This indicated that Mg/Cu-BTC@MWCNT is an adsorbent that could be potential perform very well when applied for removing CO_2 from crude syngas.

Table 3. Comparison of various MOF for CO_2 adsorption capacity.

Adsorbent	CO_2 adsorption capacity (mmol/g)	Pressure (bar)	Temperature (K)	Reference
K/Cu-BTC	8.64	18	298	[26]
MWCNT@Cu-BTC	4.3	1	298	[33]
Mg/MIL-101(Cr)	3.28	1	298	[41]
MWCNT/ MIL-101(Cr)	1.2	0.2	298	[42]
CNT/ ZIF-8	2.1	1.2	273	[43]
Mg/Cu-BTC @MWCNT	20.02	5	273	this study

Analysis of variance (ANOVA) was used to evaluate the significance of temperature and pressure on the CO_2 adsorption capacity. The resulting of Pareto diagram of standardized effect was presented in Fig.7. The confidence level of all intervals is 95%. While the adjusted R-squared value of this model is 99.79%, R-squared predicted value of 99.71%, R-squared value of 99.81%. It means that the data and the model have a very high consistency. The regression equation of this model can be expressed by Eq. (3).

$$Q = 0.134 + 0.01265\,T + 4.1130\,P - 0.04494\,T * P \quad (3)$$

Where, Q (mmol/g) is CO_2 adsorption capacity; T (K) is temperature; P (kPa) is pressure; $T * P$ is interaction between temperature and pressure.

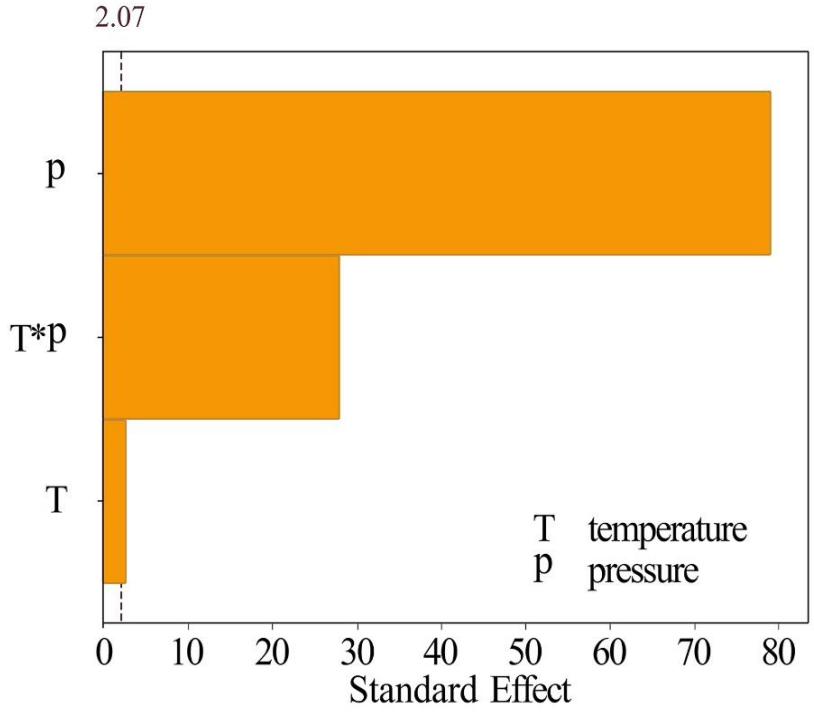

Fig.7. Pareto diagram of standard effect on CO_2 adsorption capacity.

From Pareto diagram, by comparing the significance level of the influence of adsorption pressure (P) and adsorption temperature (T) on CO_2 adsorption, pressure swing adsorption is more conducive to the effective removal of CO_2. At the same time, the synergic effect of temperature and pressure (T*P) interaction has a significantly positive influence.

3.2.2. Dynamic adsorption behavior

The process of CO_2 dynamic adsorption was investigated at 25 °C and 100 kPa, and shown in Fig.8. The adsorption dynamic equilibrium was reached as definition, when the gas adsorption rate went lower than 0.01 mmol/g·min^{-1}. The CO_2 adsorption capacity of Mg/Cu-BTC@MWCNT was about 3.63 mmol/g. The maximum adsorption rate and the maximum average adsorption rate were 0.24 mmol/g·min^{-1} and 0.16 mmol/g·min^{-1} at 16 min. In the early stages, large specific surface area and pore volume were the main reasons why the adsorbent can quickly adsorb CO_2. After 16 min, the pore channels and active sites were occupied, the adsorption rate gradually slowed down, and the adsorption capacity reached saturation at 34 min.

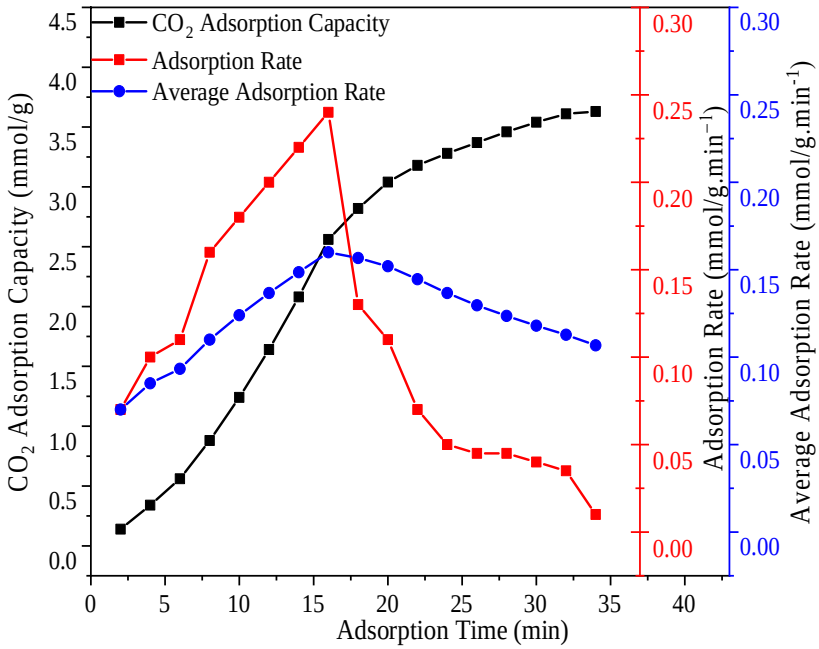

Fig.8. CO_2 adsorption capacity and adsorption rate.

3.2.3. Gas adsorption selectivity

To evaluate the adsorption behavior with syngas, CO_2/H_2 and $(CO_2+CO+CH_4)/H_2$ adsorption selectivity were calculated at 25 °C and different pressure. From Fig.9, the adsorption capacity of all of gas components increased with increasing pressure. CO_2 adsorption capacity had the most significant enhancement, from 3.63 at 100 kPa to 15.41 mmol/g at 500 kPa, while H_2 adsorption capacity only increased from 0.25 to 1.04 mmol/g. There were also small changes to the adsorption of CO and CH_4. The CO_2/H_2 selectivity showed a slight upward trend, rising from 14.28 to 14.80, this showed the influence of pressure on CO_2 adsorption is higher than H_2. However, the selectivity of $(CO_2+CO+CH_4)/H_2$ was sightly decreased from 11.52 to 11.40, this is the result of a certain amount of CO and CH_4 being adsorbed. From Fig. 9, CO adsorption capacity increased from 0.17 mmol/g to 0.83 mmol/g, and CH_4 adsorption capacity increased from 0.63 mmol/g to 1.63 mmol/g, respectively within the pressure range of 100 to 500 kPa. So, the ability of syngas components by Mg/Cu-BTC@MWCNT can be sorted as follows: CO_2> CO> CH_4> H_2. Comparing this with the selectivity of MOF in previous literatures, Mg/Cu-BTC@MWCNT had a higher CO_2/H_2 selectivity than mesoporous MCM-41 silica [44]. Based on computer simulation of zeolitic imidazolate

frameworks (ZIF) for separation of binary mixtures of CO_2, CH_4, N_2 and H_2 by a computer simulation, the result showed that CO_2/H_2 selectivity of Mg/Cu-BTC@MWCNT is higher than ZIF-10 [45]. Therefore, Mg/Cu-BTC@MWCNT is considered as a good material for H_2 purification.

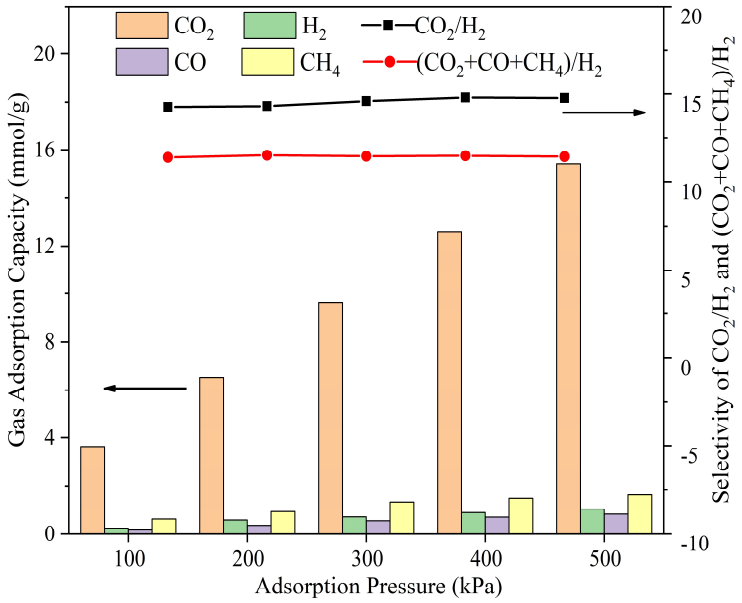

Fig.9. Gas adsorption capacity and selectivity of CO_2/H_2 and $(CO_2+CO+CH_4)/H_2$ under different adsorption pressure. Rectangle stands for adsorption capacity of each component gas; line stands for selectivity.

From the perspective of molecular electronic properties in Table 4, the large polarizability (2.9 Å) and large quadrupole moment (4.3 Å) of CO_2 have to stronger interaction forces with unsaturated metal sites in adsorbent. CH_4 have no quadrupole moment, resulting in low CH_4 adsorption capacity. H_2 adsorption of Mg/Cu-BTC@MWCNT is mainly driven only by the small molecular diameter of H_2 (2.89 Å), which entered the pores of the adsorbent through diffusion. CO_2 has a strong interaction with adsorbent, it will occupy most pore spaces and sites, therefore, H_2 adsorption capacity is limited.

Table 4. Electronic properties of H_2, CO, CH_4, CO_2.

Component	Kinetic diameter (Å)	Polarizability $(Å)^3$	Quadrupole moment $\times 10^{-10}$ $(Å)^2$
H_2	2.89	0.8042	0.662
CO	3.76	0.11	2.5
CH_4	3.8	2.6	0
CO_2	3.3	2.911	4.3

The composition changes of model syngas before and after adsorption was obtained at 25 °C and 100 kPa in Fig.10. It could be seen that CO_2 concentration decreased from 40% to 4.55%, while H_2 concentration increased from 40% to 85.9%. Compared to other syngas components, large polarizability (2.9 Å) and large quadrupole moment (4.3 Å) of CO_2 led to stronger interaction forces with unsaturated metal sites in the adsorbent. These results indicated the high adsorption capacity and high selectivity of Mg/Cu-BTC@MWCNT towards CO_2.

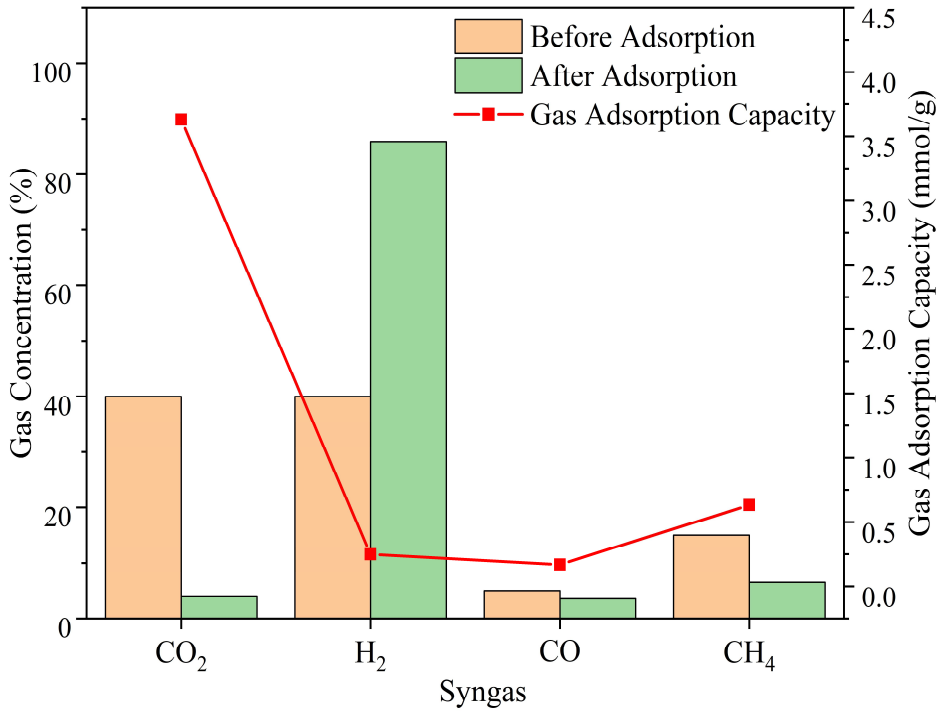

Fig.10. Changes in concentration and adsorption capacity of components of syngas.

3.2.4. Regeneration

The structural stability of adsorbent is one of the most important factors for CO_2 adsorption in industrial applications. To evaluate the structural stability of the Mg/Cu-BTC@MWCNT, CO_2 adsorption-desorption cycles were done for 5 times. Before each adsorption, the regeneration of Mg/Cu-BTC@MWCNT was conducted under N_2 atmosphere at 200 °C for 2 h. From Fig.11, the CO_2 adsorption capacity of the regenerated adsorbent was not less than 94.5% of the fresh Cu-BTC after 5 desorption cycles, suggesting the Mg/Cu-BTC@MWCNT has an excellent regeneration stability.

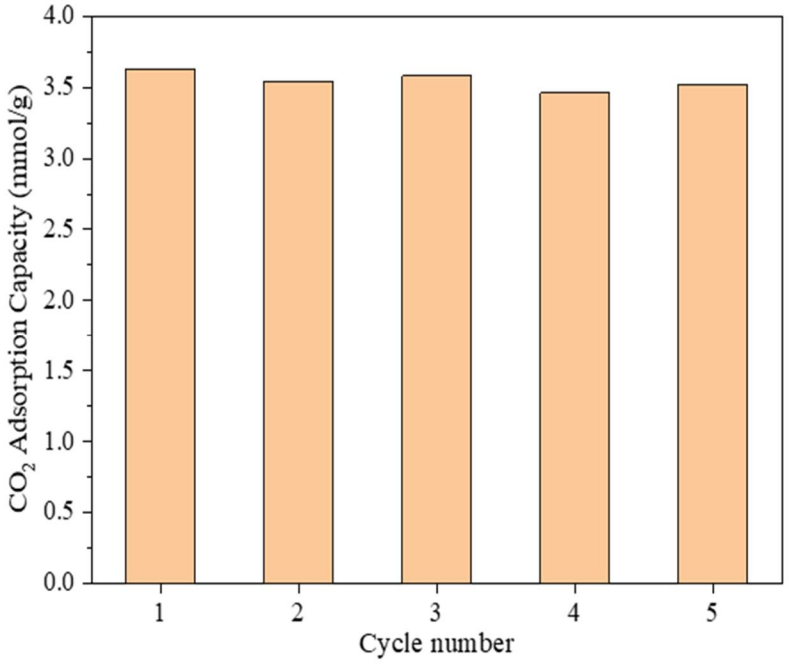

Fig.11. CO_2 adsorption capacity at 1 bar during 5 cycles.

4. Conclusion

Five different adsorbents including MWCNT, Cu-BTC, Mg/Cu-BTC, Cu-BTC@MWCNT, and Mg/Cu-BTC@MWCNT were used to investigate the performance of CO_2 adsorption from syngas. The following observations were extracted based on experiment results:

1) The doping of Mg^{2+} and MWCNT into Cu-BTC better regulated the BET surface area and pore structure. Among five adsorbents, Mg/Cu-BTC@MWCNT had the maximum CO_2 adsorption capacity with 3.63 mmol/g and adsorption selectivity with 14.28, and CO_2 concentration in model syngas decreased from 40% to 4.55% and H_2 concentration increased from 40% to 85.9% at 25 °C and 100 kPa.
2) The analysis of variance (ANOVA) indicated adsorption pressure significantly affected CO_2 adsorption capacity. While pressure has a little effect for the

improvement of selectivity Dynamic adsorption results showed the maximum adsorption rate of 0.24 mmol/g·min^{-1} was at 16 min for CO_2 adsorption on Mg/Cu-BTC@MWCNT at 25 °C and 100 kPa.

3) The regeneration experiment with 5 times presented Mg/Cu-BTC@MWCNT has high structural stability.

Generally, Mg/Cu-BTC@MWCNT had the potential for industrial application of syngas upgrading. In additional, CO_2 separated from syngas can be used in chemical compound production, modern agriculture, and oil extraction.

Credit authorship contribution statement

Yan Zhang: Investigation, Methodology, Data curation, Writing the original draft. **Haryo Wibowo:** Investigation, Methodology, Resources. **Li Zhong:** potential application analysis, **Mika Horttanainen**, Analysis improvement, Grammar writing checking, **Zunbo Wang:** Resources, Investigation, Methodology. **Caimeng Yu:** Investigation, Data curation. **Mi Yan:** Writing - review & editing, Supervision.

Conflict of interest

To the best of our knowledge, all authors have no financial interests or personal relationships that could influence work in this paper.

Acknowledgment

The authors wish to express their great appreciation of the financial support from the National Natural Science Foundation, China (51976196), and Zhejiang Natural Science Foundation Project, China (LY17E060005). At the same time, thanks to Prof Mika Horttanainen (Lappeenranta University of Technology) for the grammatical modification of this paper.

References

[1] X. Xiong, I.K.M. Yu, D.C.W. Tsang, N.S. Bolan, Y. Sik Ok, A.D. Igalavithana, M.B. Kirkham, K.H. Kim, K. Vikrant, Value-added chemicals from food supply chain wastes: State-of-the-art review and prospects, Chem. Eng. J. 375 (2019) 121983. https://doi.org/10.1016/j.cej.2019.121983.

[2] H. Su, E. Kanchanatip, D. Wang, H. Zhang, Antoni, I. Mubeen, Z. Huang, M. Yan, Catalytic gasification of food waste in supercritical water over La promoted

Ni/Al_2O_3 catalysts for enhancing H2 production, Int. J. Hydrogen Energy. 45 (2020) 553–564. https://doi.org/10.1016/j.ijhydene.2019.10.219.

[3] M.M.F. Hasan, E.L. First, F. Boukouvala, C.A. Floudas, A multi-scale framework for CO_2 capture, utilization, and sequestration: CCUS and CCU, Comput. Chem. Eng. 81 (2015) 2–21. https://doi.org/10.1016/j.compchemeng.2015.04.034.

[4] M. Yan, H. Su, Z. Zhou, D. Hantoko, E. Kanchanatip, Gasification of effluent from food waste treatment process in sub- and supercritical water: H_2-rich syngas production and pollutants management, Ence Total Environ. 730 (2020) 138517–138524. https://doi.org/10.1016/j.scitotenv.2020.138517.

[5] B. Lv, G. Jing, Y. Qian, Z. Zhou, An efficient absorbent of amine-based amino acid-functionalized ionic liquids for CO_2 capture: High capacity and regeneration ability, Chem. Eng. J. 289 (2016) 212–218. https://doi.org/10.1016/j.cej.2015.12.096.

[6] Y. Liu, P. Ghimire, M. Jaroniec, Copper benzene-1,3,5-tricarboxylate (Cu-BTC) metal-organic framework (MOF) and porous carbon composites as efficient carbon dioxide adsorbents, J. Colloid Interface Sci. 535 (2019) 122–132. https://doi.org/10.1016/j.jcis.2018.09.086.

[7] F. Wang, J. Zhao, H. Miao, J. Zhao, H. Zhang, J. Yuan, J. Yan, Current status and challenges of the ammonia escape inhibition technologies in ammonia-based CO_2 capture process, Appl. Energy. 230 (2018) 734–749. https://doi.org/10.1016/j.apenergy.2018.08.116.

[8] J. Chang, C. Hou, D. Wan, X. Zhang, B. Xu, H. Tian, X. Wang, Q. Guo, Enhanced CO_2 adsorption capacity of bi-amine co-tethered flue gas desulfurization gypsum with water of hydration, J. CO_2 Util. 35 (2020) 115–125. https://doi.org/10.1016/j.jcou.2019.09.009.

[9] F. Liu, S. Chen, Y. Gao, Synthesis of porous polymer based solid amine adsorbent: Effect of pore size and amine loading on CO_2 adsorption, J. Colloid Interface Sci. 506 (2017) 236–244. https://doi.org/10.1016/j.jcis.2017.07.049.

[10] J.T. Yeh, K.P. Resnik, K. Rygle, H.W. Pennline, Semi-batch absorption and regeneration studies for CO_2 capture by aqueous ammonia, Fuel Process. Technol. 86 (2005) 1533–1546. https://doi.org/10.1016/j.fuproc.2005.01.015.

[11] Y. Wu, Z. Lv, X. Zhou, J. Peng, Y. Tang, Z. Li, Tuning secondary building unit of Cu-BTC to simultaneously enhance its CO_2 selective adsorption and stability

under moisture, Chem. Eng. J. 355 (2019) 815–821. https://doi.org/10.1016/j.cej.2018.08.179.

[12] V.N. Le, T.K. Vo, J.H. Lee, J.C. Kim, T.-H. Kim, K.H. Oh, Y.-S. Bae, S.K. Kwak, J. Kim, A novel approach to prepare Cu(I)Zn@MIL-100(Fe) adsorbent with high CO adsorption capacity, CO/CO_2 selectivity and stability via controlled host–guest redox reaction, Chem. Eng. J. 404 (2021) 126492–126503. https://doi.org/10.1016/j.cej.2020.126492.

[13] H. Yuan, J. Chen, D. Li, H. Chen, Y. Chen, 5 Ultramicropore-rich renewable porous carbon from biomass tar with excellent adsorption capacity and selectivity for CO_2 capture, Chem. Eng. J. 373 (2019) 171–178. https://doi.org/10.1016/j.cej.2019.04.206.

[14] T. Ghanbari, F. Abnisa, W.M.A. Wan Daud, (MOF) for CO_2 adsorption:A review on production of metal organic frameworks, Sci. Total Environ. 707 (2020) 135090–135101. https://doi.org/10.1016/j.scitotenv.2019.135090.

[15] W. Chen, Z. Zhang, L. Hou, C. Yang, H. Shen, K. Yang, Z. Wang, Metal-organic framework MOF-801/PIM-1 mixed-matrix membranes for enhanced CO_2/N_2 separation performance, Sep. Purif. Technol. 250 (2020) 117198–117209. https://doi.org/10.1016/j.seppur.2020.117198.

[16] F.A. Kloutse, W. Gauthier, A. Hourri, S. Natarajan, P. Benard, R. Chahine, Study of competitive adsorption of the N_2O-CO_2-CH_4-N_2 quaternary mixture on CuBTC, Sep. Purif. Technol. 235 (2020) 116211. https://doi.org/10.1016/j.seppur.2019.116211.

[17] S. Basu, A. Cano-Odena, I.F.J. Vankelecom, MOF-containing mixed-matrix membranes for CO_2/CH_4 and CO_2/N_2 binary gas mixture separations, Sep. Purif. Technol. 81 (2011) 31–40. https://doi.org/10.1016/j.seppur.2011.06.037.

[18] P.M. Schoenecker, C.G. Carson, H. Jasuja, C.J.J. Flemming, K.S. Walton, Effect of water adsorption on retention of structure and surface area of metal-organic frameworks, Ind. Eng. Chem. Res. 51 (2012) 6513–6519. https://doi.org/10.1021/ie202325p.

[19] F. Gul-E-Noor, B. Jee, A. Pöppl, M. Hartmann, D. Himsl, M. Bertmer, Effects of varying water adsorption on a $Cu_3(BTC)_2$ metal-organic framework (MOF) as studied by 1H and 13C solid-state NMR spectroscopy, in: Phys. Chem. Chem. Phys., 17 (2011) 7783–7792. https://doi.org/10.1039/c0cp02848g.

[20] Y. Zhao, M. Seredych, J. Jagiello, Q. Zhong, T.J. Bandosz, Insight into the mechanism of CO_2 adsorption on Cu-BTC and its composites with graphite oxide or aminated graphite oxide, Chem. Eng. J. 239 (2014) 399–407. https://doi.org/10.1016/j.cej.2013.11.037.

[21] S.C. Qi, X.Y. Qian, Q.X. He, K.J. Miao, Y. Jiang, P. Tan, X.Q. Liu, L.B. Sun, Generation of Hierarchical Porosity in Metal–Organic Frameworks by the Modulation of Cation Valence, Angew. Chemie - Int. Ed. 58 (2019) 10104–10109. https://doi.org/10.1002/anie.201903323.

[22] S. Qiu, J. Du, Y. Xiao, Q. Zhao, G. He, Hierarchical porous HKUST-1 fabricated by microwave-assisted synthesis with CTAB for enhanced adsorptive removal of benzothiophene from fuel, Sep. Purif. Technol. 271 (2021) 118868. https://doi.org/10.1016/j.seppur.2021.118868.

[23] X.-Y. Xie, X.-Y. Qian, S.-C. Qi, J.-K. Wu, X.-Q. Liu, L.-B. Sun, Endowing Cu-BTC with Improved Hydrothermal Stability and Catalytic Activity: Hybridization with Natural Clay Attapulgite via Vapor-Induced Crystallization, ACS Sustain. Chem. Eng. 6 (2018) 13217–13225. https://doi.org/10.1021/acssuschemeng.8b02827.

[24] A.A.. G. and M.J. Yuanyuan Lu, Sugin Liu, Effect of metal-ligand ratio on the CO_2 adsorption properties of Cu-BTC metal-organic frameworks, R. Soc. Chem. 8 (2018) 35551-35558. https://doi.org/10.1039/C8RA07774F.

[25] N. Wang, A. Mundstock, Y. Liu, A. Huang, J. Caro, Amine-modified Mg-MOF-74/CPO-27-Mg membrane with enhanced H_2/CO_2 separation, Chem. Eng. Sci. 124 (2015) 27–36. https://doi.org/10.1016/j.ces.2014.10.037.

[26] Y. Cao, Y. Zhao, F. Song, Q. Zhong, Alkali metal cation doping of metal-organic framework for enhancing carbon dioxide adsorption capacity, J. Energy Chem. 23 (2014) 468–474. https://doi.org/10.1016/S2095-4956(14)60173-X.

[27] H. Sun, T. Wang, Y. Xu, W. Gao, P. Li, Q.J. Niu, Fabrication of polyimide and functionalized multi-walled carbon nanotubes mixed matrix membranes by in-situ polymerization for CO_2 separation, Sep. Purif. Technol. 177 (2017) 327–336. https://doi.org/10.1016/j.seppur.2017.01.015.

[28] S. C. Hsu, C. Lu, F. Su, W. Zeng, W. Chen, Thermodynamics and regeneration studies of CO_2 adsorption on multiwalled carbon nanotubes, Chem. Eng. Sci. 65 (2010) 1354–1361. https://doi.org/10.1016/j.ces.2009.10.005.

[29] Z. Z. Zhu, Z. Wang, H. L. Li, Functional multi-walled carbon

nanotube/polyaniline composite films as supports of platinum for formic acid electrooxidation, Appl. Surf. Sci. 254 (2008) 2934–2940. https://doi.org/10.1016/j.apsusc.2007.10.033.

[30] M. Anbia, S. Sheykhi, Preparation of multi-walled carbon nanotube incorporated MIL-53-Cu composite metal-organic framework with enhanced methane sorption, J. Ind. Eng. Chem. 19 (2013) 1583–1586. https://doi.org/10.1016/j.jiec.2013.01.026.

[31] M. Konni, S. Doddi, A.S. Dadhich, S.B. Mukkamala, Adsorption of CO_2 by hierarchical structures of f-MWCNTs@Zn/Co-ZIF and N-MWCNTs@Zn/Co-ZIF prepared through in situ growth of ZIFs in CNTs, Surfaces and Interfaces. 12 (2018) 20–25. https://doi.org/10.1016/j.surfin.2018.04.006.

[32] S.J. Yang, J.Y. Choi, H.K. Chae, J.H. Cho, K.S. Nahm, C.R. Park, Preparation and enhanced hydrostability and hydrogen storage capacity of CNT©MOF-5 hybrid composite, Chem. Mater. 21 (2009) 1893–1897. https://doi.org/10.1021/cm803502y.

[33] F. Eshraghi, M. Anbia, S. Salehi, Dative post synthetic methods on SBUs of MWCNT@MOFs hybrid composite and its effect on CO_2 uptake properties, J. Environ. Chem. Eng. 5 (2017) 4516–4523. https://doi.org/10.1016/j.jece.2017.08.040.

[34] Z. Xiang, Z. Hu, D. Cao, W. Yang, J. Lu, B. Han, W. Wang, Metal-Organic Frameworks with Incorporated Carbon Nanotubes: Improving Carbon Dioxide and Methane Storage Capacities by Lithium Doping, Angew. Chemie Int. Ed. 50 (2011) 491–494. https://doi.org/10.1002/anie.201004537.

[35] Nadeen. Al-Janabi, PatrickHill, LauraTorrente-Murciano, ArthurGarforth, PatriciaGorgojo, FlorSiperstein, XiaoleiFan, Mapping the Cu-BTC metal-organic framework (HKUST-1) stability envelope in the presence of water vapour for CO_2 adsorption from flue gases, Chem. Eng. J. 281 (2015) 669–677. https://doi.org/10.1016/j.cej.2015.07.020.

[36] J.-M. Lee, S.J. Kim, J.W. Kim, P.H. Kang, Y.C. Nho, Y.-S. Lee, A high resolution XPS study of sidewall functionalized MWCNTs by fluorination, J. Ind. Eng. Chem. 15 (2009) 66–71. https://doi.org/10.1016/j.jiec.2008.08.010.

[37] M. Klimakow, P. Klobes, K. Rademann, F. Emmerling, Characterization of mechanochemically synthesized MOFs, Microporous Mesoporous Mater. 154 (2012) 113–118. https://doi.org/10.1016/j.micromeso.2011.11.039.

[38] Y. Yang, H. Dong, Y. Wang, C. He, Y. Wang, X. Zhang, Synthesis of octahedral like Cu-BTC derivatives derived from MOF calcined under different atmosphere for application in CO oxidation, J. Solid State Chem. 258 (2018) 582–587. https://doi.org/10.1016/j.jssc.2017.11.033.

[39] S. Xu, H. Huang, X. Guo, Z. Qiao, C. Zhong, Highly selective gas transport channels in mixed matrix membranes fabricated by using water-stable Cu-BTC, Sep. Purif. Technol. 257 (2021) 117979–117985. https://doi.org/10.1016/j.seppur.2020.117979.

[40] Enin, P. Jakubczak, M. Lanuza, D.B. Galloway, J.J. Low, R.R. Willis, Screening of metal-organic frameworks for carbon dioxide capture from flue gas using a combined experimental and modeling approach, J. Am. Chem. Soc. (2009). https://doi.org/10.1021/ja9057234.

[41] Z. Zhou, L. Mei, C. Ma, F. Xu, J. Xiao, Q. Xia, Z. Li, A novel bimetallic MIL-101(Cr, Mg) with high CO_2 adsorption capacity and CO_2/N_2 selectivity, Chem. Eng. Sci. 147 (2016) 109–117. https://doi.org/10.1016/j.ces.2016.03.035.

[42] N.A.A. Qasem, N.U. Qadir, R. Ben-Mansour, S.A.M. Said, Synthesis, characterization, and CO_2 breakthrough adsorption of a novel MWCNT/MIL-101(Cr) composite, J. CO_2 Util. 22 (2017) 238–249. https://doi.org/10.1016/j.jcou.2017.10.015.

[43] Y. Yang, L. Ge, V. Rudolph, Z. Zhu, In situ synthesis of zeolitic imidazolate frameworks/carbon nanotube composites with enhanced CO_2 adsorption, Dalt. Trans. 43 (2014) 7028–7036. https://doi.org/10.1039/C3DT53191K.

[44] Y. Belmabkhout, A. Sayari, Adsorption of CO_2 from dry gases on MCM-41 silica at ambient temperature and high pressure. 2: Adsorption of CO_2/N_2, CO_2/CH_4 and CO_2/H_2 binary mixtures, Chem. Eng. Sci. 64 (2009) 3729–3735. https://doi.org/10.1016/j.ces.2009.05.039.

[45] A. Battisti, S. Taioli, G. Garberoglio, Zeolitic imidazolate frameworks for separation of binary mixtures of CO_2, CH_4, N_2 and H_2: A computer simulation investigation, Microporous Mesoporous Mater. 143 (2011) 46–53. https://doi.org/10.1016/j.micromeso.2011.01.029.